



# Preparation of $\alpha$ -zirconium phosphate-pillared reduced graphene oxide with increased adsorption towards methylene blue



Zhimin Wu<sup>a,b</sup>, Li Zhang<sup>b</sup>, Qingqing Guan<sup>c</sup>, Ping Ning<sup>c</sup>, Daiqi Ye<sup>a,d,e,\*</sup>

<sup>a</sup> College of Environment and Energy, South China University of Technology, Guangzhou 510006, China

<sup>b</sup> Department of Light Chemistry Engineering, Guangdong Polytechnic, Foshan 528041, China

<sup>c</sup> Faculty of Environmental Science and Engineering, Kunming University of Science and Technology, Kunming 650093, China

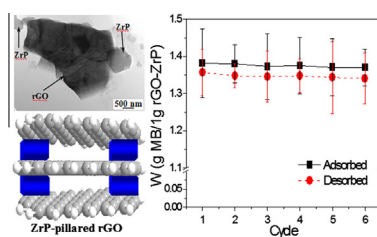
<sup>d</sup> Guangdong Provincial Key Laboratory of Atmospheric Environment and Pollution Control (SCUT), Guangzhou 510006, China

<sup>e</sup> Guangdong High Education Engineering Technology Research Center for Air Pollution Control, Guangzhou 510006, China

## HIGHLIGHTS

- $\alpha$ -Zirconium phosphate (ZrP) pillared reduced graphene oxide (rGO) was prepared.
- rGO-ZrP possessed a higher BET specific surface area than rGO.
- The reunion of rGO-ZrP was interrupted by ZrP during storage.
- The maximum adsorption capacity of MB onto rGO-ZrP was  $\sim 1.38$  g/g at 30 °C.
- Adsorption-desorption efficiency of rGO-ZrP remained constant after six cycles.

## GRAPHICAL ABSTRACT



## ARTICLE INFO

### Article history:

Received 28 May 2014

Received in revised form 13 July 2014

Accepted 14 July 2014

Available online 22 July 2014

### Keywords:

Reduced graphene oxide  
 $\alpha$ -Zirconium phosphate  
Pillared  
Adsorption  
Methylene blue

## ABSTRACT

In order to prevent the reunion of reduced graphene oxide (rGO) during storage,  $\alpha$ -zirconium phosphate (ZrP) was used as the modifier, and a peculiar adsorbent of ZrP-pillared rGO (rGO-ZrP) was prepared. The features of rGO-ZrP were characterized by using Fourier transform infrared (FTIR), scanning electron microscope (SEM), transmission electron microscopy (TEM), energy dispersion X-ray (EDX) spectrometer, atomic force microscopy (AFM) and X-ray diffraction (XRD) measurements. Then, rGO-ZrP was employed as the adsorbent and the adsorption characteristics of rGO-ZrP toward methylene blue (MB) were evaluated under laboratory conditions. The results showed that rGO-ZrP possessed a higher BET specific surface area relative to rGO. The maximum adsorption quantity of MB onto the new prepared rGO-ZrP was  $\sim 1.38$  g/g at 30 °C. With the increase of storage day, the BET specific surface area and the maximum adsorption capacity of rGO-ZrP approximately remained unchanged. Under the maximum adsorption capacity, the adsorption quantity of MB onto rGO-ZrP was dependent on the initial concentration of MB, and higher temperature could facilitate the adsorption process. The efficiency of rGO-ZrP almost remained constant during the first six cycles of adsorption-desorption process. In addition, the fluorescence spectra implied that the adsorption of MB onto rGO-ZrP was a  $\pi$ - $\pi$  stacking adsorption process, and the pillared structure of rGO-ZrP greatly enhanced the noncovalent adhesion. In conclusion, rGO-ZrP could serve as a promising adsorbent for the removal of MB in waste water.

Crown Copyright © 2014 Published by Elsevier B.V. All rights reserved.

\* Corresponding author at: College of Environment and Energy, South China University of Technology, Guangzhou 510006, China. Tel.: +86 20 39380502.

E-mail address: [cedqye@scut.edu.cn](mailto:cedqye@scut.edu.cn) (D. Ye).

## 1. Introduction

Dyes have become one of the main sources of severe water pollution as a result of the rapid development of the textile industry and their low production costs, brighter color, strong resistance towards environmental factor and easy-to-apply factor [1,2]. Among them, methylene blue (MB) has the widest application, which includes coloring paper, temporary hair colourant, dyeing cotton, wool and coating for paper stock. The presence of dye in water, even at very low concentration, is highly visible and undesirable [3].

In the past years, several technologies have been employed for the removal of heavy metals and dyes from aqueous solution, such as adsorption, ion exchange, chemical precipitation and membrane separation [4–6]. Among them, adsorption is the simplest and the most cost-effective technique. In addition, adsorption does not result in secondary pollution by producing harmful substance during the process [7]. Numerous works have presented results for the adsorption of dyes onto various materials like activated carbon, natural and synthetic polymer, montmorillonite and its modified composite, clay, zeolite, biomass, and agricultural and industrial by-product [8–11].

In the past few years, graphene have attracted tremendous interest in the world. Some reviews on graphene-based material as adsorbent for the removal of pollutant are available [6,12]. Compared to other carbon-based materials, the advantage of the use of graphene is the adsorption ability to chemicals with benzene rings through strong  $\pi$ - $\pi$  interaction [6]. The selective adsorption ability will make graphene serve as a promising adsorbent for the removal of chemicals containing benzene rings in waste water. The main shortcomings of graphene are the easy agglomeration during storage, which result in the decline of adsorption capacity in practical application. In order to solve the problem, physical [13] or chemical [14,15] modification of graphene or graphene oxide (GO) was used, but the results are still not ideal. Therefore, it is necessary to probe new methods which can solve the agglomeration problem.

Zirconium bis-(monohydrogen orthophosphate) monohydrate ( $\text{Zr}(\text{HPO}_4)_2 \cdot \text{H}_2\text{O}$ ), also called layered  $\alpha$ -zirconium phosphate (ZrP), is drawing increasing attention because of its ability to serve as ion exchanger, catalyst and carrier of intercalation [16,17]. With self-organized lamellar structure and abundant hydroxyl group, ZrP has the potential to be used as carrier for functional materials because of its high exchange capability and excellent absorptive performance.

In this study, ZrP was used as the modifier, and a peculiar adsorbent of ZrP-pillared reduced graphene oxide (rGO-ZrP) was prepared. The methylene blue (MB) was chosen as a typical dye, and the adsorption properties of rGO-ZrP were evaluated under laboratory conditions. As a new type of material, rGO-ZrP combined the properties of rGO and ZrP, and behaved higher adsorption efficiency than rGO after long-term storage.

## 2. Materials and methods

### 2.1. Materials

Zirconium oxychloride octahydrate ( $\text{ZrOCl}_2 \cdot 8\text{H}_2\text{O}$ , 98%) and phosphoric acid ( $\text{H}_3\text{PO}_4$ , 85%, v/v) were obtained from Sigma-Aldrich (Shanghai, China). Graphite powder (spectral pure),  $\text{KMnO}_4$ ,  $\text{P}_2\text{O}_5$ , concentrated  $\text{H}_2\text{SO}_4$ ,  $\text{H}_2\text{O}_2$  and MB were purchased from Sinopharm Chemical Reagent Co., Ltd. (Shanghai, China). Hydrazine monohydrate (50 wt% in water) was purchased from Aladdin reagent Inc. (Shanghai, China). All MB aqueous solutions used in this study were prepared by dissolving a certain amount

of MB in ultrapure water. All other reagents and solvents were obtained from commercial suppliers. All aqueous solutions were prepared with ultrapure water ( $>18 \text{ M}\Omega \text{ cm}$ ) from a Milli-Q Plus system (Millipore).

### 2.2. Preparation of GO and ZrP

GO was synthesized from natural graphite powder by a modified Hummers method [18–21]. The ZrP was synthesized by hydrothermal method. Briefly,  $\text{ZrOCl}_2 \cdot 8\text{H}_2\text{O}$  was dissolved in deionized water with stir. Then, the solution was slowly added into phosphoric acid ( $\text{H}_3\text{PO}_4$ ) to produce a sol-gel. The resultant sol-gel was put into a round-bottomed flask, and hydrothermally treated at  $120^\circ\text{C}$  with reflux condenser for 7 days. After cooling to room temperature, the aggregates were filtered, washed with ultrapure water until the neutral pH, and dried in vacuum at  $65^\circ\text{C}$  for 24 h.

### 2.3. Fabrication of rGO-ZrP

The rGO-ZrP was prepared as follows: 2 g ZrP intercalated with saturated methylamine [22] was dispersed in 50 mL ultrapure water, to which 1 g GO was slowly added. Then, the reaction mixture was sonicated vigorously at  $60^\circ\text{C}$  for 6 h (KQ218, 60 W). After that, 250 mL hydrazine monohydrate (50 wt% in water) was added and the mixture was reacted at  $85^\circ\text{C}$  for 48 h. Finally, a homogeneous incanus dispersion was obtained. The resulting solution was then filtered through a polycarbonate membrane ( $0.22 \mu\text{m}$  of pore size) and repeatedly washed by ultrapure water. After freeze-dried, the powder was put into a semi-closed alumina crucible with a cover. The crucible was heated at  $450^\circ\text{C}$  for 100 min (heating rate of  $2^\circ\text{C min}^{-1}$ ) to burn the chemicals away. After cooling to room temperature, the obtained product was named as rGO-ZrP.

### 2.4. Characterization

Fourier transform infrared (FTIR) spectra were measured with a Bruker Vertex 70 FTIR spectrophotometer using the KBr method. The morphology of the sample was observed by scanning electron microscope (SEM) and transmission electron microscope (TEM) using PHILIPS XL-30 scanning electron microscopy and Philips TECNAI-10 transmission electron microscopy, respectively. Energy dispersive X-ray (EDX) spectra were measured with an Oxford ISIS-300 EDX spectrometer. X-ray diffraction (XRD) patterns were obtained on a PANalytical's X'Pert Power X-ray Diffraction (40 kV, 30 mA) with  $\text{Cu K}\alpha$  radiation at a scanning rate of  $2.4^\circ/\text{min}$ . A continuous scan mode was applied to collect  $2\theta$  data from  $2^\circ$  to  $40^\circ$ . Atomic Force Microscopy (AFM) images were observed by an atomic force microscope (Benyuan CSPM5500) on a flat mica substrate. Fluorescence spectra were detected by a Hitachi F4600 fluorescence spectrophotometer. BET (Brunauer-Emmett-Teller) specific surface area was determined using Micromeritics ASAP 2010 instrument. Thermogravimetric analysis (TGA) was conducted with a thermal analyzer (NETZSCH TG 209) under  $\text{N}_2$  flow, and the temperature range of the measurements was  $40$ – $900^\circ\text{C}$  and the scanning rate was  $10^\circ\text{C}/\text{min}$ .

### 2.5. Adsorption experiment

The adsorption tests of MB onto the rGO-ZrP were conducted in batch experiment at  $30^\circ\text{C}$ . A series of 100 mL solution in 250 mL flask were used and each flask was filled with rGO-ZrP at various mass loadings (0.05–0.3 g) and MB solution at different initial concentrations. The flasks were agitated in an orbital shaker at 150 rpm and treated at a given time interval. The suspension was centrifuged at 4500 rpm for 10 min to separate liquid from solid

phase, and then the supernatant liquid was analyzed for MB. MB was determined spectrophotometrically by measuring the absorbance at 664 nm (Spectronic 20 Genesys Spectrophotometer). The pH values of the samples were adjusted by adding 0.1 mol/L HCl or NaOH, and were measured using a pH meter (METTLER TOLEDO, FE20).

At equilibrium, the adsorbed amount of MB per unit mass of adsorbent ( $q_e$ , mg/g) was determined according to the following mass balance:

$$q_e = \frac{(C_0 - C_e)V}{M} \quad (1)$$

where  $V$  was the liquid volume (L),  $C_0$  was the initial concentration (mg/L),  $C_e$  was the equilibrium concentration (mg/L), and  $M$  was the amount of the adsorbent MB onto a dry basis (g), respectively. To evaluate the maximum adsorption capacity and the adsorption–desorption property of rGO–ZrP, 0.1 g of rGO–ZrP was put into a conical flask containing 100 mL of MB aqueous solution (5 g/L). The flask was covered well and shaken in the water bath shaker at 30 °C for 4 days. Then, the adsorbed rGO–ZrP was filtered using 0.22  $\mu\text{m}$  membrane filter, and heated at 450 °C for 100 min to burn the chemicals away. The adsorption–desorption process was repeated for six times. The adsorption capacity was the difference between the initial and final concentration of MB aqueous solution, and the desorption capacity was the difference between the initial and final weight of the adsorbed rGO–ZrP.

### 3. Results and discussion

#### 3.1. Characterization of rGO–ZrP

The FTIR spectroscopy was carried out for confirming the chemical composition of the prepared composite. According to the FTIR spectrum of ZrP (Fig. 1a), the bands at 3595, 3510 and 3155  $\text{cm}^{-1}$  were due to the –OH stretching mode of P–OH of ZrP structure; the bands at 1250 and 595  $\text{cm}^{-1}$  were caused by the stretching vibration of in-plane deformation vibration of P–OH; the strong bands near 988 and 966  $\text{cm}^{-1}$  were probably caused by the stretching vibration of P–O in the infrared spectra, according to MacLanchian [23]. Therefore, we could determine the chemical composition of ZrP was  $\alpha\text{-Zr}(\text{HPO}_4)_2 \cdot \text{H}_2\text{O}$ .

In the FTIR spectrum of GO (Fig. 1b), a broad and intensive peak appeared at 3430  $\text{cm}^{-1}$  was assigned to –OH stretching band, which might originate from water molecules adsorbed inside GO. Besides, peaks at 1726, 1622, 1385 and 1052  $\text{cm}^{-1}$  corresponded to C=O, C–OH, C=C and C–O–C vibration frequencies, respectively. These peaks suggested that graphite had been already oxidized to GO [24]. As GO was reduced to rGO (Fig. 1c), the adsorption bands of oxygen functionalities disappeared and only the peaks at 1052 and 1622  $\text{cm}^{-1}$  remained, which was similar to that of pristine graphite. In the FTIR spectrum of rGO–ZrP (Fig. 1d), all peaks of rGO and ZrP appeared, and the bands of peaks belonging to rGO and ZrP became weak. These results illustrated that rGO had been composited with ZrP, and rGO–ZrP was indeed obtained.

The representative SEM image of ZrP was shown in Fig. 2a. Fig. 2b showed the EDX spectrum of ZrP, revealing that ZrP contained elements of O, P and Zr, which meant it was  $\alpha\text{-Zr}(\text{HPO}_4)_2 \cdot \text{H}_2\text{O}$  [25]. The representative SEM image of rGO–ZrP was shown in Fig. 2c. The rGO–ZrP contained a mass of particles on the surface and in the interlayer sheets of rGO, which suggested to be ZrP. The layered structure of rGO–ZrP exhibited a much rougher surface, which would provide more active sites for the adsorption of dye or heavy metal ion and help to enhance the adsorption activity of rGO–ZrP. Fig. 2d showed the EDX spectrum of rGO–ZrP, revealing

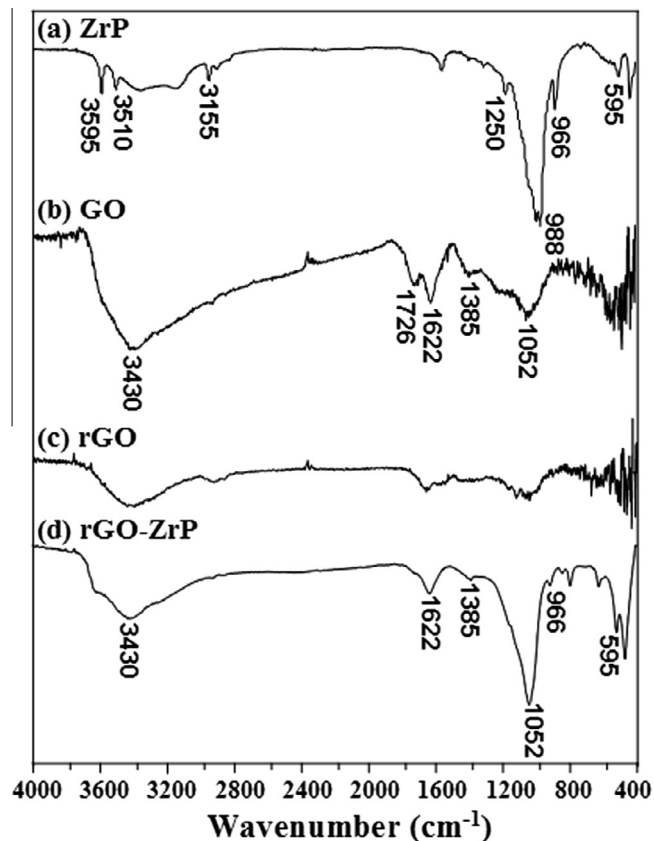


Fig. 1. The FTIR spectra of ZrP (a), GO (b), rGO (c) and rGO–ZrP (d).

that rGO–ZrP contained elements of C, O, P and Zr. The presences of O, P and Zr atoms corroborated the existence of ZrP, and the element of C could be related to rGO.

The XRD patterns were presented in Fig. 3. For ZrP, a typical diffraction peak at  $2\theta = 11.71^\circ$  corresponded to a basal spacing ( $d_{002}$ ) of 0.76 nm (Fig. 3a) [25]. For GO, the peak at  $2\theta = 9.3^\circ$ , corresponding to the interlayer spacing of 0.950 nm (Fig. 3c), might be due to high degree of exfoliation and disordered structure of GO. For rGO, the peak at  $2\theta = 24.8^\circ$  represented the interlayer spacing of 0.359 nm (Fig. 3d). This value was slightly larger than that of graphite, which was mainly due to the residual functional groups that might exist between the rGO layers.

In order to increase the layer spacing of ZrP, ZrP was firstly intercalated by methylamine. As shown in Fig. 3b, the diffraction peak emerged at lower  $2\theta$  value of  $7.31^\circ$ , corresponding to the increased  $d_{002}$  basal spacing of 1.21 nm. The results implied that methylamine was intercalated into the interlayer of ZrP, which increased the interlamellar spacing of ZrP. For rGO–ZrP before heat treating, a new peak centered at  $2\theta = 5.52^\circ$ , corresponding to the  $d_{002}$  basal spacing of 1.60 nm (Fig. 3e), might be due to the intercalation of rGO into the layer spacing of methylamine intercalated ZrP. As for rGO–ZrP, the characteristic peak of rGO–ZrP before heat treating disappeared, and a well-defined new peak appeared at  $7.61^\circ$  with 1.16 nm  $d_{002}$  basal spacing (Fig. 3f), which might be ascribed that the heat treating burned the methylamine away, resulting in the ZrP-pillared rGO.

In order to further illustrate the above XRD results, TEM and AFM were used. As shown in Fig. 4a, ZrP had well-ordered layered structure. The surface of ZrP particles was smooth, and the size of ZrP was about 0.2–0.5  $\mu\text{m}$  (length)  $\times$  0.1–0.5  $\mu\text{m}$  (width). As shown in Fig. 4b, the ultrasonic treatment of rGO kept some singer layer in solution, and the thickness of singer layer rGO was about

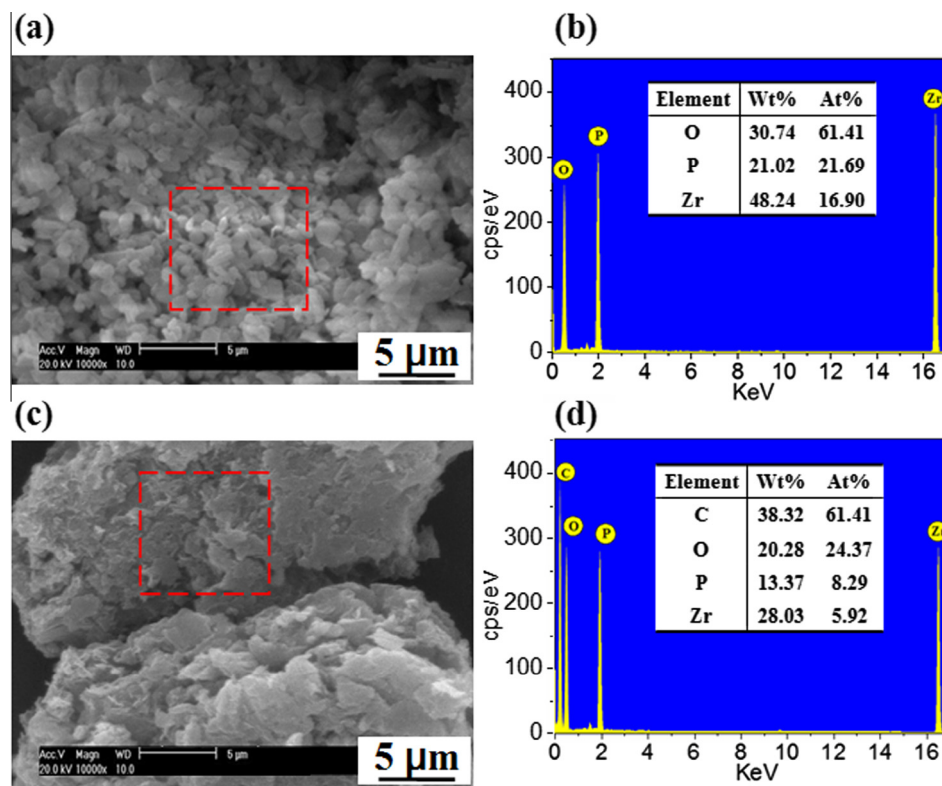


Fig. 2. SEM micrographs of ZrP (a) and rGO-ZrP (c); EDX spectra of ZrP (b) and rGO-ZrP (d).

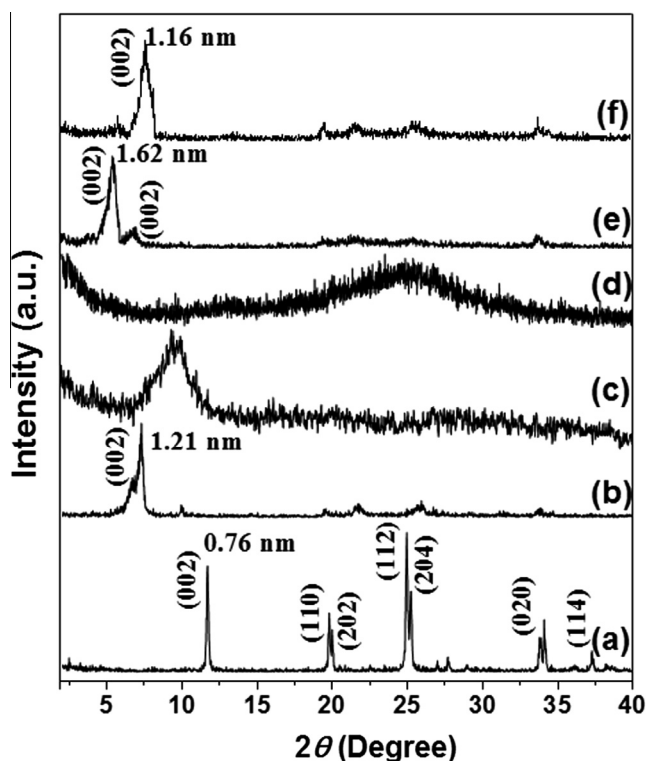


Fig. 3. XRD patterns of (a) ZrP, (b) ZrP intercalated with saturated methylamine, (c) GO, (d) rGO, (e) rGO-ZrP before heat treating, and (f) rGO-ZrP.

0.4 nm which depended on the degree of deoxidation [26]. The size of ZrP was about 3–4 μm (length) × 2–3 μm (width).

As shown in Fig. 4c, the small size of particle was ZrP and the large size of particle was rGO, since the characteristic peak of

rGO disappeared (Fig. 4c). Moreover, some small particles were pillared into the rGO (Fig. 4c). We suggested that ZrP pillared the rGO, and rGO-ZrP (Fig. 4d) was got. This insinuation was consistent with the SEM, EDX and XRD results.

As shown in Fig. 5, the BET specific surface area of rGO-ZrP and rGO were 573 and 312 m<sup>2</sup> g<sup>-1</sup>, respectively. The discrepancy on as-obtained data and theoretical value of surface area of rGO (2620 m<sup>2</sup> g<sup>-1</sup>) was attributed to the incomplete exfoliation and aggregation during reduction process because of the unavoidable van der Waals force between each single layer of rGO. The higher BET specific surface area of rGO-ZrP relative to rGO was due to the pillar of rGO by ZrP. With the increase of storage day, for example, after 120 days, the BET specific surface area of rGO was decreased to 44 m<sup>2</sup> g<sup>-1</sup>, while the BET specific surface area of rGO-ZrP was only decreased to 523 m<sup>2</sup> g<sup>-1</sup>. π-π bonding interaction had been used to interpret this phenomenon. Since the rGO contained π electrons to interact with the π electrons of the nearby rGO through the π-π electron coupling [27,28], rGO would reunite with the increase of storage day, while the reunion of rGO-ZrP was interrupted by ZrP. These results showed that ZrP could increase the storage stability.

### 3.2. Adsorption speed and capacity of MB on rGO-ZrP and rGO

rGO-ZrP and rGO expressed different adsorption speeds and different maximum adsorption capacities for MB. As could be seen from Fig. 6a, for rGO-ZrP, the concentration of MB was sharply decreased at the first 10 min from 250 mg/L to below 37 mg/L; for rGO, the concentration of MB was decreased at the first 10 min from 250 mg/L to below 69 mg/L. With the passage of time, the slope of rGO-ZrP was larger than rGO, which meant that rGO-ZrP expressed faster adsorption speeds than rGO. The physisorption of organic molecule was a noncovalent functionalization involving π-stacking interaction and corresponding to a weak

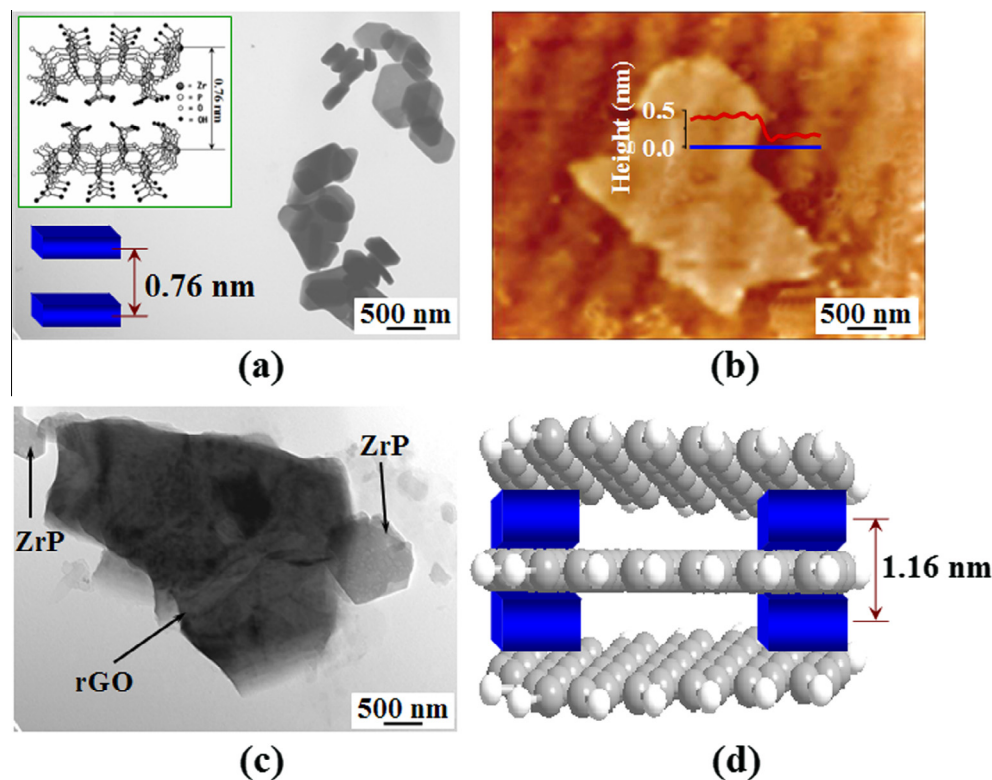


**Fig. 4.** (a) TEM image of ZrP, (b) Tapping-mode AFM image of rGO on a clean mica surface and cross-sectional profile of GO indicated by a blue line, (c) the TEM image of rGO-ZrP, and (d) the schematic of rGO-ZrP. (For interpretation of the references to color in this figure legend, the reader is referred to the web version of this article.)

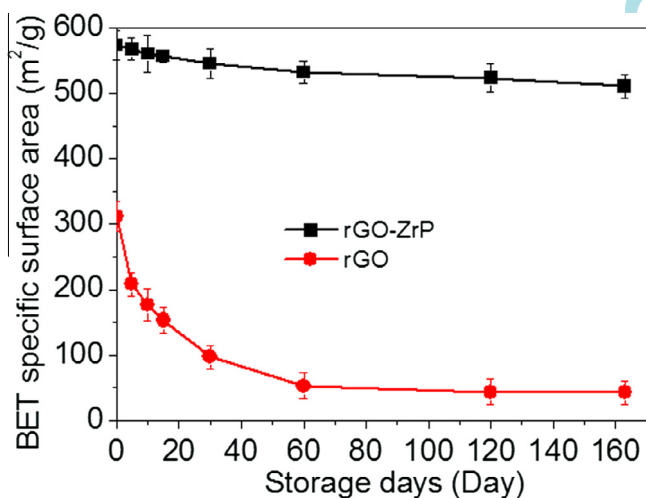


**Fig. 5.** The BET specific surface areas of rGO-ZrP and rGO with different storage days.

binding energy. The  $\pi$ - $\pi$  bonding interaction between rGO (or rGO-ZrP) and MB was affected by the BET specific surface area. Since rGO-ZrP had larger BET specific surface area than rGO, rGO-ZrP expressed faster adsorption speeds than rGO.

As could be seen from Fig. 6b, the maximum adsorption capacities of MB onto the rGO and rGO-ZrP were  $\sim 0.73$  g/g rGO and  $\sim 1.38$  g/g rGO-ZrP at 30 °C. With the increase of storage days in water, the maximum adsorption capacities of MB onto the rGO was dramatic decreased to  $\sim 0.09$  g/g rGO at 30 °C, while the maximum adsorption capacities of MB onto the rGO-ZrP was only decreased to  $\sim 1.21$  g/g rGO-ZrP at 30 °C. The results might be related to the reunite of rGO in water, while the reunite of

rGO-ZrP in water was interrupted by ZrP, which was consistent with the result of BET specific surface area.

### 3.3. Effects of the initial concentration and adsorption time on adsorption of MB onto the rGO-ZrP

The effects of the initial concentrations and adsorption time on adsorption of MB onto the rGO-ZrP were shown in Fig. 7. It could be seen that the concentrations of MB in all initial concentration experiments was decreased sharply at the first 10 min, and then reduced slowly until the adsorption equilibrium was reached after 60 min. These results indicated that under the maximum adsorption capacity, the adsorption quantity of MB onto the rGO-ZrP was dependent on the initial concentration of MB [27,28].

### 3.4. Effect of temperature and pH on adsorption of MB onto the rGO-ZrP

The effect of temperature on adsorption was shown in Fig. 8a. After 30 min, the concentration of MB was decreased from the initial concentration of 250 mg/L to 25, 24 and 19 mg/L, respectively under the temperatures of 20, 30 and 40 °C. It seemed that higher temperature facilitated the adsorption of MB onto the rGO-ZrP. The increase of temperature might produce a swelling effect within the internal structure of adsorbent, penetrating the large dye molecule further [29]. Standard free energy change ( $\Delta G_0$ ) provided information about the interaction between the surface of rGO-ZrP and the MB. The  $\Delta G_0$  could be calculated from the relationship [30]:

$$\Delta G_0 = RT \ln K_d \quad (2)$$

where  $R$  was the universal gas constant ( $8.314 \text{ J mol}^{-1} \text{ K}^{-1}$ ),  $T$  was the temperature in Kelvin, and the distribution adsorption coefficient,  $K_d$ , was calculated from the following equation:

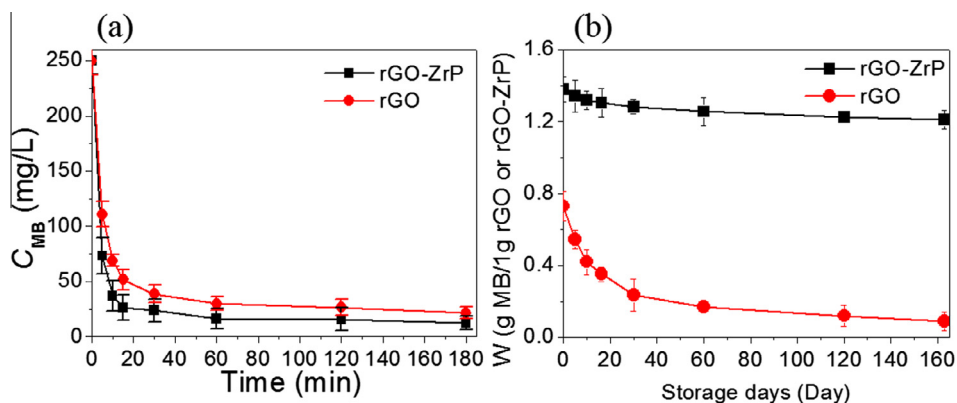


Fig. 6. (a) Adsorption characteristics of MB onto the rGO-ZrP and rGO; (b) maximum adsorption capacities of MB onto the rGO-ZrP and rGO.

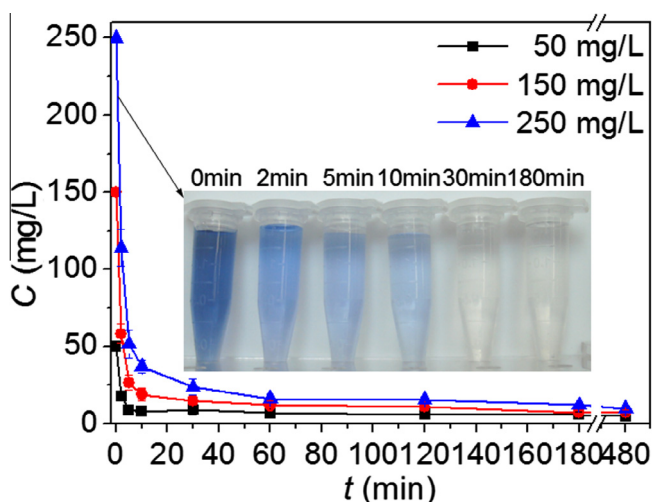


Fig. 7. Effects of the initial concentration and adsorption time on adsorption of MB onto the rGO-ZrP.

$$K_d = \frac{C_0 - C_e}{C_e} \cdot \frac{V}{m} \quad (3)$$

where  $C_0$  was the initial concentration (mmol/L),  $C_e$  was the equilibration concentration after centrifugation (mmol/L),  $V$  was the volume (L) of the suspension, and  $m$  was the mass of adsorbent (g). The adsorption equilibrium constant,  $K_0$ , could be calculated by plotting  $\ln K_d$  versus  $C_e$  and extrapolating  $C_e$  to zero. The value of the intercept was that of  $\ln K_0$ .

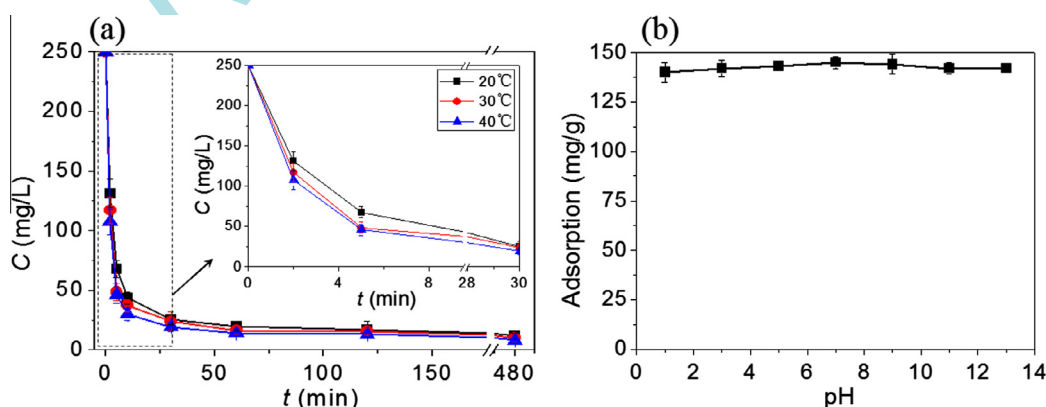


Fig. 8. (a) Effect of the temperature on adsorption of MB onto the rGO-ZrP; (b) effect of the pH on adsorption of MB onto the rGO-ZrP.

$\Delta G^0$  values calculated from Eqs. 2 and 3 were listed in Table 1.

The negative  $\Delta G^0$  indicated that the adsorption was a spontaneous process. Moreover, the value of  $\Delta G^0$  became more negative with the increase of temperature, indicating that the adsorption process was more favorable at higher temperature.

It is well-known that the pH of the system was an important variable in the adsorption process. Fig. 8b showed the variation of adsorption of MB (150 mg/L) on rGO-ZrP at various pH values. It demonstrated that the rGO-ZrP had a good adsorption capacity in acid range, and the highest adsorption kept nearly constant between 2 and 11. Similar results was also report [31].

### 3.5. Adsorption–desorption property of rGO-ZrP

In order to better explain the reasons that the maximum adsorption capacity of rGO-ZrP almost remained constant during the first six cycles of adsorption–desorption process, the TGA test and BET test were used to explain this results instead of adsorption isotherms. The TGA curves of rGO-ZrP and MB/rGO-ZrP were showed in Fig. 9a. The decomposition of rGO-ZrP clearly occurred in two general regions below 900 °C: (1) evaporation of free (absorbed) and interlayer water residing between the layers and comprising the hydration spheres of the cations was between 50–200 °C; (2) dehydroxylation of the ZrP and rGO lattice was between 500 and 700 °C. By contrast, the TGA curves of MB/rGO-ZrP might be conveniently divided into three regions [17]: (1) desorption of absorbed water and gases was below 200 °C; (2) decomposition of the MB was between 200 and 500 °C; (3) dehydroxylation of the ZrP and rGO lattice was between 500 and 700 °C. So, 450 °C was used to burn the MB away.

**Table 1**  
 $\Delta G^0$  of MB adsorption on rGO-ZrP at 20, 30 and 40 °C.

	20 °C/293.15 K	30 °C/303.15 K	40 °C/313.15 K
$\Delta G^0$ (kJ mol <sup>-1</sup> )	-10.19	-10.73	-11.25

With regard to the efficiency evolution of rGO-ZrP during adsorption–desorption cycles, it could be seen in Fig. 9b that during six cycles, no appreciable change in the amount of adsorbed MB was found, and each value agreed with its corresponding desorbed quantity (within experimental error of (2%)). We also test the BET specific surface areas of rGO-ZrP during six cycles, and the BET specific surface area of rGO-ZrP were 573, 554, 547, 551, 553, and 549 m<sup>2</sup> g<sup>-1</sup> after six cycles, respectively. That meant the regeneration of rGO-ZrP was complete under the working conditions and the efficiency of rGO-ZrP almost remained constant during, at least, the first six cycles of the adsorption–desorption process.

### 3.6. Adsorption mechanism

In order to reveal the dominant adsorption mechanism of MB onto the rGO-ZrP, XRD patterns and fluorescence spectra were used. According to XRD pattern, the (002) interlayer spacing of

rGO-ZrP shifted from 1.16 nm to 2.54 nm after adsorption of MB onto the rGO-ZrP (Fig. 10a). This could be explained by the intercalation of MB molecule into the interlayer of rGO-ZrP. Each carbon atom in rGO-ZrP sheet had a  $\pi$  electron orbit which was perpendicular to the surface of rGO-ZrP, so organic molecules containing  $\pi$  electrons, such as organic molecules with C=C double bonds and benzene rings, could form  $\pi$ - $\pi$  bond with rGO-ZrP. The quenching phenomenon could be used as an indicator of trans-annular  $\pi$ - $\pi$  interaction [32]. Therefore, the fluorescence spectra of MB and MB/rGO-ZrP (rGO-ZrP adsorbed by MB) in water were recorded.

As shown in Fig. 10b, MB had a strong emission with the maximum at 689 nm, and the significant quenching of the MB fluorescence by rGO-ZrP was caused by effective photoinduced charge transfer between MB and rGO-ZrP [33,34]. Given the chemical structure of MB, we could speculate that the intermolecular force between MB and rGO-ZrP might be  $\pi$ - $\pi$  stacking interaction. Moreover, the complete quenching of the MB fluorescence in MB/rGO-ZrP revealed that MB and rGO-ZrP closely stacked in a compact manner, and finally formed a thin-layer object (Fig. 10c). These results suggested the strong  $\pi$ - $\pi$  stacking interaction between the benzene rings of MB and the rGO-ZrP surface, and the pillared structure of rGO-ZrP greatly enhanced the noncovalent adhesion.

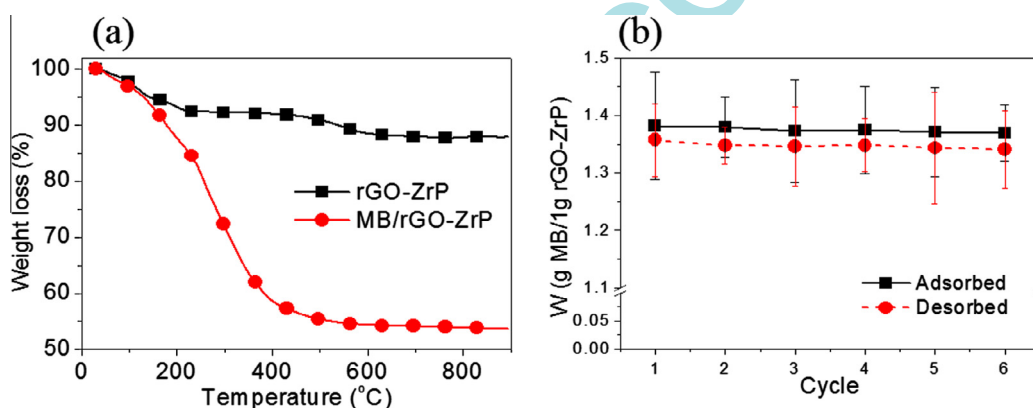


**Fig. 9.** (a) TGA curves of rGO-ZrP and MB/rGO-ZrP; (b) adsorbed and desorbed quantities (g MB/g rGO-ZrP) for six cycles using rGO-ZrP as adsorbate ( $n = 3$ ,  $\pm$ SD).

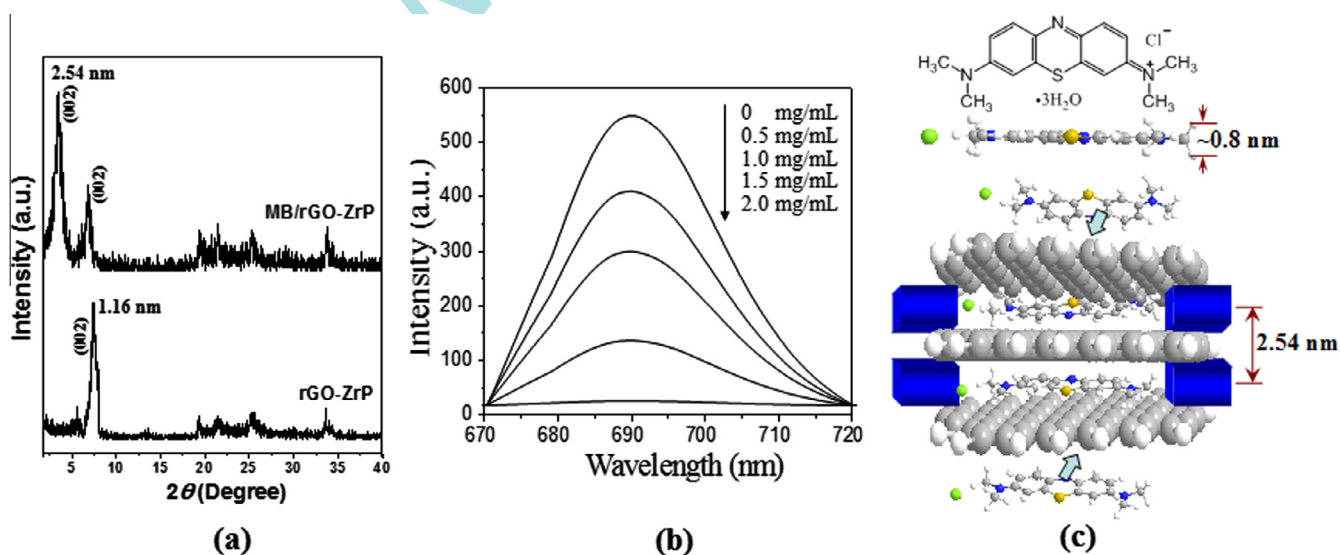


**Fig. 10.** (a) XRD patterns of rGO-ZrP and the rGO-ZrP adsorbed by MB (MB/rGO-ZrP); (b) fluorescence spectra of MB (1.6 mg/L) upon gradual addition of rGO-ZrP (0–2.0 mg/L) in aqueous solution with an excitation wavelength of 660 nm (25 °C); (c) the schematic of  $\pi$ - $\pi$  interactions between the MB and the surface of rGO-ZrP.

#### 4. Conclusion

In this study, ZrP-pillared rGO as a peculiar adsorbent was prepared. Due to the pillar of rGO by ZrP, the BET specific surface area of rGO–ZrP ( $573 \text{ m}^2 \text{ g}^{-1}$ ) was higher than that of rGO ( $312 \text{ m}^2 \text{ g}^{-1}$ ). The rGO reunited with the increase of storage day, while the reunite of rGO–ZrP was interrupted by ZrP. The rGO–ZrP behaved faster adsorption speeds than rGO, and the maximum adsorption capacity of MB onto the new prepared rGO–ZrP was  $\sim 1.38 \text{ g/g}$  at  $30^\circ \text{C}$ . The absorption quantity of MB onto the rGO–ZrP was dependent on the initial concentration of MB. Moreover, the negative  $\Delta G^0$  indicated that the adsorption was a spontaneous process and higher temperature could facilitate the adsorption process. The efficiency of rGO–ZrP almost remained constant during the first six cycles of the adsorption–desorption process. The fluorescence spectra implied that the adsorption of MB onto the rGO–ZrP was a  $\pi$ – $\pi$  stacking adsorption process. The results were important to understand the potential application of rGO–ZrP in environmental pollution management.

#### Acknowledgments

This work was financially supported by the National Natural Science Foundation of China (No. U1137603), and the 2013 higher education institution Outstanding Young Teachers Funding Scheme of Guangdong Province (No. Yq2013173).

#### References

- [1] B. Prelot, V. Einhorn, F. Marchandeu, J.M. Douillard, J. Zajac, Bulk hydrolysis and solid–liquid sorption of heavy metals in multi-component aqueous suspensions containing porous inorganic solids: are these mechanisms competitive or cooperative?, *J Colloid Interface Sci.* 386 (2012) 300–306.
- [2] L. Campbell, D.G. Dixon, R.E. Hecky, A review of mercury in Lake Victoria, East Africa: implications for human and ecosystem health, *J. Toxicol. Environ. Health* 6 (2003) 325–356.
- [3] T. Wu, X. Cai, S.Z. Tan, H.Y. Li, J.S. Liu, W.D. Yang, Adsorption characteristics of acrylonitrile, p-toluenesulfonic acid, 1-naphthalenesulfonic acid and methyl blue on graphene in aqueous solutions, *Chem. Eng. J.* 173 (2011) 144–149.
- [4] S.K. Porter, K.G. Scheckel, C.A. Impellitteri, J.A. Ryan, Toxic metals in the environment: thermodynamic considerations for possible immobilization strategies for Pb, Cd, As, and Hg, *Crit. Rev. Environ. Sci. Technol.* 34 (2004) 495–604.
- [5] J.L. Gardea-Torresdey, G. de la Rosa, J.R. Peralta-Videa, Use of phytoremediation technologies in the removal of heavy metals: a review, *Pure Appl. Chem.* 76 (2004) 801–813.
- [6] M. Pansini, Nature zeolites as cation exchangers for environmental protection, *Miner. Deposita* 31 (1996) 563–575.
- [7] S.B. Wang, T. Terdkiatburana, M.O. Tadé, Single and co-adsorption of heavy metals and humic acid on fly ash, *Sep. Purif. Technol.* 58 (2008) 353–358.
- [8] S.J. Allen, G. McKay, J.F. Porter, Adsorption isotherm models for basic dye adsorption by peat in single and binary component systems, *J. Colloid Interface Sci.* 280 (2004) 322–333.
- [9] M.Y. Chang, R.S. Juang, Adsorption of tannic acid, humic acid, and dyes from water using the composites of chitosan and activated clay, *J. Colloid Interface Sci.* 278 (2004) 18–25.
- [10] A. Bhatnagar, A.K. Jain, A comparative adsorption study with different industrial wastes as adsorbents for the removal of cationic dyes from water, *J. Colloid Interface Sci.* 281 (2005) 49–55.
- [11] V.K. Gupta, A. Mittal, V. Gajbe, Adsorption and desorption studies of a water soluble dye, Quinoline Yellow, using waste materials, *J. Colloid Interface Sci.* 284 (2005) 89–98.
- [12] S.B. Wang, H.Q. Sun, H.M. Ang, M.O. Tadé, Adsorptive remediation of environmental pollutants using novel graphene-based nanomaterials, *Chem. Eng. J.* 226 (2013) 336–347.
- [13] D. Ma, J.T. Lin, Y.Y. Chen, W. Xue, L.M. Zhang, In situ gelation and sustained release of an antitumor drug by graphene oxide nanosheets, *Carbon* 50 (2012) 3001–3007.
- [14] A. Sahu, W.I. Choi, G. Tae, A stimuli-sensitive injectable graphene oxide composite hydrogel, *Chem. Commun.* 48 (2012) 5820–5822.
- [15] Z.Y. Sui, Y. Cui, J.H. Zhu, B.H. Han, Preparation of three-dimensional graphene oxide-polyethylenimine porous materials as dye and gas adsorbents, *ACS Appl. Mater. Interfaces* 5 (2013) 9172–9179.
- [16] X. Cai, G.J. Dai, S.Z. Tan, Y. Ouyang, Y.S. Ouyang, Q. Shi, Synergistic antibacterial zinc ions and cerium ions loaded  $\alpha$ -zirconium phosphate, *Mater. Lett.* 67 (2012) 199–201.
- [17] M. Karlsson, C. Andersson, J. Hjortkjaer, Hydroformylation of propene and 1-hexene catalysed by a  $\alpha$ -zirconium phosphate supported rhodium–phosphine complex, *J. Mol. Catal. A Chem.* 166 (2001) 337–343.
- [18] C.M. Chen, Q.H. Yang, Y.G. Yang, W. Lv, Y.F. Wen, P.X. Hou, M.Z. Wang, H.M. Cheng, Self-assembled free-standing graphite oxide membrane, *Adv. Mater.* 21 (2009) 3007–3011.
- [19] X. Cai, S.Z. Tan, A.G. Xie, M.S. Lin, Y.L. Liu, X.J. Zhang, Z.D. Lin, T. Wu, W.J. Mai, Conductive methyl blue-functionalized reduced graphene oxide with excellent stability and solubility in water, *Mater. Res. Bull.* 46 (2011) 2353–2358.
- [20] X. Cai, S.Z. Tan, M.S. Lin, A.G. Xie, W.J. Mai, X.J. Zhang, Z.D. Lin, T. Wu, Y.L. Liu, Synergistic antibacterial brilliant blue/reduced graphene oxide/quaternary phosphonium salt composite with excellent water-solubility and specific-targeting capability, *Langmuir* 27 (2011) 7828–7835.
- [21] X. Cai, S.Z. Tan, A.L. Yu, J.L. Zhang, J.H. Liu, W.J. Mai, Z.Y. Jiang, Sodium 1-naphthalenesulfonate-functionalized reduced graphene oxide stabilize the silver nanoparticles with lower cytotoxicity and long-term antibacterial activity, *Chem. Asian J.* 7 (2012) 1664–1670.
- [22] L. Sun, W.J. Boo, A. Clearfield, H.-J. Sue, Preparation of exfoliated epoxy/ $\alpha$ -zirconium phosphate nanocomposites containing high aspect ratio nanoplatelets, *Chem. Mater.* 19 (2007) 1749–1754.
- [23] D.J. MacLachlan, K.R. Morgan, Phosphorus-31 solid-state NMR studies of the structure of amine-intercalated,  $\alpha$ -zirconium phosphate. 2. Titration of  $\alpha$ -zirconium phosphate with n-propylamine and n-butylamine, *J. Phys. Chem.* 96 (1992) 3458–3464.
- [24] X. Cai, M.S. Lin, S.Z. Tan, W.J. Mai, Y.M. Zhang, Z.W. Liang, Z.D. Lin, X.J. Zhang, The use of polyethyleneimine-modified reduced graphene oxide as a substrate for silver nanoparticles to produce a material with lower cytotoxicity and long-term antibacterial activity, *Carbon* 50 (2012) 3407–3415.
- [25] H.H. Murray, Applied Clay Mineralogy: Occurrences, Processing and Applications of Kaolins, Bentonites, Palygorskite-Sepiolite, and Common Clays, Elsevier, 2006. pp. 23–47.
- [26] D. Pandey, R. Reifemberger, R. Piner, Scanning probe microscopy study of exfoliated oxidized graphene sheets, *Surf. Sci.* 602 (2008) 1607–1613.
- [27] C. Namasivayam, N. Muniasamy, K. Gayathri, M. Rani, K. Ranganathan, Removal of dyes from aqueous solutions by cellulosic waste orange peel, *Bioresour. Technol.* 57 (1996) 37–43.
- [28] C. Namasivayam, D. Kavitha, Removal of Congo Red from water by adsorption onto activated carbon prepared from coir pith, an agricultural solid waste, *Dyes Pigm.* 54 (2002) 47–58.
- [29] K.G. Bhattacharyya, A. Sarma, Adsorption characteristics of the dye, Brilliant Green, on Neem leaf powder, *Dyes Pigm.* 57 (2003) 211–222.
- [30] X. Yang, S.B. Yang, S.T. Yang, J. Hu, X.L. Tan, X.K. Wang, Effect of pH, ionic strength and temperature on sorption of Pb(II) on NKF-6 zeolite studied by batch technique, *Chem. Eng. J.* 168 (2011) 86–93.
- [31] G.K. Ramesha, A.V. Kumara, H.B. Muralidhara, S. Sampath, Graphene and graphene oxide as effective adsorbents toward anionic and cationic dyes, *J. Colloid Interface Sci.* 361 (2011) 270–277.
- [32] W.L. Wang, J.W. Xu, Z. Sun, X.H. Zhang, Y. Lu, Y.H. Lai, Effect of transannular  $\pi$ – $\pi$  interaction on emission spectral shift and fluorescence quenching in dithia[3.3] paracyclophane-fluorene copolymers, *Macromolecules* 39 (2006) 7277–7285.
- [33] X. Qi, K.Y. Pu, X. Zhou, H. Li, B. Liu, F. Boey, W. Huang, H. Zhang, Conjugated-polyelectrolyte-functionalized reduced graphene oxide with excellent solubility and stability in polar solvents, *Small* 6 (2010) 663–669.
- [34] Z. Yang, X. Shi, J. Yuan, H. Pu, Y. Liu, Preparation of poly(3-hexylthiophene)/graphene nanocomposite via in situ reduction of modified graph-ite oxide sheets, *Appl. Surf. Sci.* 257 (2010) 138–142.